Impact of Water Film Thickness on Kinetic Rate of Mixed Hydrate Formation During Injection of CO_2 into CH_4 Hydrate

Khuram Baig, Bjørn Kvamme, Tatiana Kuznetsova, and Jordan Bauman
Dept. of Physics and Technology, University of Bergen, NO-5020 Bergen, Norway

DOI 10.1002/aic.14913
Published online July 14, 2015 in Wiley Online Library (wileyonlinelibrary.com)

In this work, nonequilibrium thermodynamics and phase field theory (PFT) has been applied to study the kinetics of phase transitions associated with CO_2 injection into systems containing CH_4 hydrate, free CH_4 gas, and varying amounts of liquid water. The CH_4 hydrate was converted into either pure CO_2 or mixed CO_2—CH_4 hydrate to investigate the impact of two primary mechanisms governing the relevant phase transitions: solid-state mass transport through hydrate and heat transfer away from the newly formed CO_2 hydrate. Experimentally proven dependence of kinetic conversion rate on the amount of available free pore water was investigated and successfully reproduced in our model systems. It was found that rate of conversion was directly proportional to the amount of liquid water initially surrounding the hydrate. When all of the liquid has been converted into either CO_2 or mixed CO_2—CH_4 hydrate, a much slower solid-state mass transport becomes the dominant mechanism. © 2015 American Institute of Chemical Engineers *AIChE J*, 61: 3944–3957, 2015

Keywords: natural gas hydrates, nonequilibrium thermodynamics, mixed hydrate, phase field theory

Introduction

Natural gas hydrates are ice-like crystalline compounds in which water serve as a host for different small nonpolar, or slightly polar guest molecules. Natural gas hydrates occur both onshore in permafrost regions and continental margin sediments consisting mainly of fine-grained clay minerals and organic fragments. The majority of natural gas hydrate deposits existing around the world are found in fine-grained sediments characterized by low-hydrate saturation, which can be explained by very small pore size and low permeability of clay-rich sediments that hinder mobility of both water and gas, components essential for formation of hydrate. Gas hydrates mostly occur in sand units and are largely absent from mud sequences.[1–3]

Permafrost gas hydrate occurrences have been identified in sand-rich deposits in on-shore and near-shore environments, with gas hydrate deposits in Alaska and Canada being the typical examples. Analysis of well log data[4] and pore water geochemistry[5] indicates a very level of hydrate saturation at the Mount Elbert site (about 60–75%), which can be attributed to pre-existing free gas and presence of high conductivity faults.[6]

Natural gas hydrates are dominated by biogenic sources of methane. Indeed, according to Michael et al.,[7] as much as 99% of all gas hydrate deposits may be of biogenic origin. In contrast to natural gas of thermogenic origin, biogenic methane is very pure and contains only tiny amounts of heavier hydrocarbons. In this work, we, therefore, focus on hydrates of methane and carbon dioxide and their mixtures, known to form hydrates of structure I.[8,9]

Hydrate formation from methane and water can follow a number of different pathways. The most commonly discussed route is hydrate formation on the interface between the hydrate-former phase and water.[8] Numerous experimental data are available in literature (see, for instance, Koh and Sloan[10] for a compilation), though it should be pointed that the bulk of data[10] comes from dissociation point measurements, where hydrate is kept at a controlled pressure and slowly increasing temperature.

But hydrate can also form from hydrate formers dissolved in water[11,12] and (theoretically) from water dissolved in the hydrate-former phase,[13] although more comprehensive analysis is still needed to decide whether the latter route is realistic under mass- and heat-transport limitations. Earlier theoretical studies[14–21] indicate that the critical hydrate nucleus will be about 2.5–3 nm in size, which would require around a hundred of water molecules to come together within a very dilute mixture in natural gas or carbon dioxide. Even then, the excess heat of hydrate formation will be rather difficult to dispose of, since both natural gas and carbon dioxide are thermal insulators.

Mineral surfaces[13,22,23] will serve as adsorption sites for water and hydrate formers, which can give rise to at least three different formation scenarios even in the simplest case: (1) water and hydrate former, both from adsorbed phase, form hydrate, (2) adsorbed water and hydrate fluid forms hydrate, and (3) adsorbed hydrate former and water from fluid phase forms hydrate. Considering all the possible phases relevant for hydrate formation, hydrate dissociation, and hydrate reformation (CH_4 hydrate over to CO_2 hydrate or mixed CO_2/CH_4 hydrate), it will be impossible to satisfy the Gibbs phase rule

Correspondence concerning this article should be addressed to B. Kvamme at Bjorn.Kvamme@ift.uib.no

and for the system to achieve equilibrium. But even in this case, the equality of chemical potentials at the asymptotic equilibrium limit will still provide the driving forces during hydrate formation that will affect the hydrate filling and corresponding hydrate free energy.

Since the system will be generally unable to reach equilibrium, the dynamic situation will be governed by the combined first and second laws of thermodynamics under mass- and heat-transport constraints. This indicates that a proper analysis of competing phase transitions will required some sort of free energy minimization scheme. The phase field theory (PFT)[14–21] is a theoretical method very well suited for this task. It should be mentioned that the first layers of adsorbed water might have too low chemical potential to form hydrate but few (2–4) water molecules outside will have chemical potentials suitable for hydrate formation.[22]

Injection of carbon dioxide into methane hydrate will lead to conversion of in situ methane hydrate into a mixed hydrate where carbon dioxide dominates the large cavities and methane fills a fraction of the small cavities. This rate of this conversion is governed by two main mechanisms. Formation of new carbon dioxide hydrate from residual pore water will release heat that contributes to dissociation of surrounding methane hydrate. A second mechanism is a substantially slower direct solid-state exchange.[24,25] This hydrate exchange is also feasible with injection of carbon dioxide and nitrogen mixtures, as demonstrated by the Prudhoe Bay field pilot project in the winter of Ref. 26.

In this work, we use an extended version of PFT[14–21] incorporating both hydrodynamics and heat transport, developed and discussed in detail elsewhere.[14–50] The need to include the hydrodynamic effects arises when the rate of hydrate dissociation is so high that released methane is unable to dissolve fully into the surrounding water and forms bubbles affecting phase transition kinetics. Transport of heat released by hydrate will normally be 2–3 orders of magnitude faster than mass transport in a liquid water/hydrate system.[14–21] Heat transport will, however, be slow through gas layers or gas bubbles. Implicit treatment of heat transport will, therefore, be necessary when formation of new hydrate contributes to dissociation of original methane hydrate. Extension of thermodynamic properties to regions outside of equilibrium is quite trivial for the fluid phases, with the pertinent equations provided in the next section along with the equilibrium hydrate treatment. We then proceed to extend the hydrate thermodynamics beyond the equilibrium region using Taylor expansion of the first order.

Equilibrium thermodynamics

The theory for equilibrium thermodynamics is based on revised adsorption theory by Kvamme and Tanaka[8] and van der Waals and Platteeuw.[27] The expression for chemical potential of water in hydrate is

$$\mu_w^{\mathrm{H}} = \mu_w^{\mathrm{O,H}} - \sum_i RTv_i \ln\left(1+\sum_j h_{ij}\right) \tag{1}$$

This equation is derived from the macrocanonical ensemble under the constraints of constant amount of water, corresponding to an empty lattice of the actual structure. Details of the derivation are given elsewhere (Kvamme and Tanaka[8]) and will not be repeated here. $\imath_w^{\mathrm{O,H}}$ is the chemical potential for water in an empty hydrate structure and h_{ij} is the cavity partition function of component j in cavity type i. The first sum is over cavity types, and the second sum is over components j going into cavity type i. Here v_i is the number of type i cavities per water molecule. For hydrate Structure I, there are three large cavities and one small per 23 water molecules, $v_{\mathrm{l}} = 3/23$ and $v_{\mathrm{s}} = 1/23$. In the classical use of Eq. 1, the cavity partition functions are integrated under the assumption that the water molecules are fixed and normally also neglecting interactions with surrounding guest molecules. This may be adequate for small guest molecules with weak interactions. Conversely, molecules like CO_2 are large enough to have a significant impact on the librational modes of the water molecules in the lattice. An alternative approach[8] is to consider the guest movements from the minimum energy position in the cavity as a spring, and evaluate the free energy changes through samplings of frequencies for different displacements in the cavity. A molecule like methane will, as expected, not have significant impact on the water movements.[8,51] CO_2, conversely, will change water chemical potential by roughly 1 kJ/mole at 0°C when compared to the assumption of undisturbed fixed water molecules. The cavity partition function may thus be written as

$$h_{ij} = \mathrm{e}^{\beta\left(\mu_j^H - \Delta g_{ji}^{\mathrm{inc}}\right)} \tag{2}$$

where Δg_{ji}^{inc} now is the effect of the inclusion of the guest molecule j in the cavity of type i, which as indicated above is the minimum interaction energy plus the free energy of the oscillatory movements from the minimum position. At hydrate equilibrium, the chemical potential is equal to that of the chemical potential of the guest molecule in its original phase (chemical potential of dissolved CO_2 or CH_4 for the case of hydrate formation from aqueous solution). Equation 2 can be inverted to give the chemical potential for the guest as a function of the cavity partition function

$$\mu_j^{\mathrm{H}} = \Delta g_{ji}^{\mathrm{inc}} + RT\ln h_{ij} \tag{3}$$

Equation 3 is basically derived from an equilibrium consideration but may be used as an approximation for bridging chemical potential to composition dependency. The relation between the filling fraction, the mole fractions and the cavity partition function is

$$\theta_{ji} = \frac{x_{ji}}{v_i(1-x_{\mathrm{T}})} = \frac{h_{ji}}{1+\sum_j h_{ji}} \tag{4}$$

here x_{T} is the total mole fraction of all the guests. It is assumed that CO_2 can only fit into the larger cavities, and unless some other guest molecule is present, the small cavities will then all be empty. For a system with only one component occupying the large cavities, the chemical potential of the guest molecule would be reduced to

$$\mu_w^{\mathrm{H}} = \Delta g_{ji}^{\mathrm{inc}} + RT\ln\left(\frac{\theta_{ji}}{1-\theta_{ji}}\right) \tag{5}$$

For methane, which can occupy both large and small cavities, a more cumbersome approach is needed. Initially assuming that chemical potential of methane in the two cavities is the same. This gives a proportional relation between the two partition functions independent on composition

$$\frac{h_{m\mathrm{l}}}{h_{m\mathrm{s}}} = e^{\left(\frac{\Delta g_{m\mathrm{s}}^{\mathrm{inc}} - \Delta g_{m\mathrm{l}}^{\mathrm{inc}}}{RT}\right)} = A \tag{6}$$

The mole fraction of methane x_m is the sum of the mole fraction in each cavity, that is, large $x_{m\mathrm{l}}$ and small $x_{m\mathrm{s}}$. The

mole fractions are expressed in terms of the cavity partition function from Eq. 4

$$x_{ms}+x_{ml}=x_m \tag{7}$$

$$\frac{h_{ms}}{1+h_{ms}}v_s+\frac{h_{ml}}{1+h_{ml}+h_{cl}}v_l=\frac{x_m}{1+x_T}=B \tag{8}$$

here h_{ms}, h_{ml}, and h_{cl} are the cavity partition functions of methane in small cavities, methane in large cavities, and carbon dioxide in large cavities, respectively. The denominator in the second term can be expressed in terms of the mole fraction and one of the partition functions from Eqs. 4 and 7

$$1+h_{ml}+h_{ms} \tag{9}$$

The partition function for CO_2 using Eqs. 4 needs to be calculated as:

$$\frac{x_{cl}}{v_l(1-x_T)}=\frac{h_{cl}}{1+h_{ml}+h_{cl}}$$

Rearranging the above equation in term of h_{cl} gives:

$$h_{cl}=\frac{x_{cl}(1+h_{ml})}{v_l(1-x_T)-x_{cl}}$$

Inserting the value of h_{cl} in Eq. 9, which gives constant C

$$1+h_{ml}+h_{cl}=(1+h_{ml})\left(1+\frac{x_{cl}}{v_l(1-x_T)-x_{cl}}\right) \tag{10}$$

$$C=1+\frac{x_{cl}}{v_l(1-x_T)-x_{cl}} \tag{11}$$

Using Eqs. 6, 10, and 11 results

$$1+h_{ml}+h_{cl}=(1+Ah_{ms})C \tag{12}$$

Equation 8 can be written in terms of single partition function

$$\frac{h_{ms}}{1+h_{ms}}v_s+\frac{Ah_{ms}}{(1+Ah_{ms})C}v_l=B \tag{13}$$

Equation 13 can be simplified to yield a second-order equation

$$(v_sCA+v_lA-BCA)h_{ms}^2+(v_sC+v_lA-BCA-BC)h_{ms}-BC=0 \tag{14}$$

Equation 14 can be written in the form of second constant

$$a_1(h_{ms})^2+a_2(h_{ms})+a_3=0 \tag{15}$$

$$a_1=A(v_l+v_sC-BC)$$

$$a_2=v_sC+Av_l-BC(1+A)$$

$$a_3=-BC$$

Fluid thermodynamic

The free energy of the fluid phase is assumed to have

$$G_L^{\text{Fluid}}=\sum_{r=c,m,w}x_r\mu_r^{\text{Fluid}} \tag{16}$$

where μ_r^{Fluid} is the chemical potentials of the fluid phase components. The lower concentration of water in the fluid phase and its corresponding minor importance for the thermodynamics results in the following form of water chemical potential with some approximation of fugacity and activity coefficient

$$\mu_w^{\text{Fluid}}=\mu_w^{\text{ideal gas}}(T,P)+RT\ln(y_w) \tag{17}$$

where $\mu_w^{\text{ideal gas}}(T,P)$ chemical potential of water in ideal gas and y_w is the mole fraction of water in the fluid phase and can be calculated as

$$y_w=\frac{x_w\gamma_w(T,P,\bar{x})P_w^{\text{sat}}(T)}{\varphi_w(T,P,\bar{y})} \tag{18}$$

The vapor pressure can be calculated using many available correlations but one of the simplest is given in Refs. 29 and 54 as a fit to the simple equation

$$\ln(P)=V_A-\frac{V_B}{T+V_C} \tag{19}$$

The temperature of the system is obviously available and $V_A=52.703$, $V_B=-3146.64$, and $V_C=5.572$. Further, the fugacity and the activity coefficient are approximated to unity merely because of the very low-water content in fluid phase and its corresponding minor importance for the thermodynamics of the system. Hydrate formation directly from water in gas is not considered as significant within the systems discussed in this work. A separate study reveals that hydrate formation from water dissolved in carbon dioxide may be feasible from a thermodynamic point of view[29] but more questionable in terms of mass transport in competition with other hydrate-phase transitions. The water phase is close to unity in water mole fraction. Raoult's law is, therefore, accurate enough for our purpose. The chemical potential for the mixed fluid states considered as

$$\mu_i^{\text{Fluid}}=\mu_i^{\text{id.gas, pure}}+RT\ln(y_i)+RT\ln\varphi_i(T,P,\bar{y}) \tag{20}$$

where i represents CH_4 or CO_2. The fugacity coefficients of component i in the mixture is calculated using the Soave–Redlich–Kwong (SRK) equation of state (EOS)[15,30,51]

$$\ln\varphi_i=(BB)_i(Z-1)-\ln(Z-B)-\frac{A}{B}\left((AA)_i-(BB)_i\right)\ln\left[1+\frac{B}{Z}\right] \tag{21}$$

where Z is the compressibility factor of the phase and is calculated using the following cubic SRK EOS

$$Z^3-Z^2+\left(A-B-B^2\right)Z-AB=0 \tag{22}$$

where

$$A=\frac{\alpha aP}{R^2T^2}$$

$$B=\frac{bP}{RT}$$

$$a=0.427480\frac{R^2T_c^2}{P_c}$$

$$b=0.086640\frac{RT_c}{P_c}$$

$$\alpha=\left[1+\left(0.48508+1.55171\omega-0.15613\omega^2\right)\left(1-\sqrt{T_r}\right)\right]^2$$

where ω is the accentric factor of components. For mixture, the mixing rule with modification proposed by Soave[30] is used using the following formulations

$$(\alpha a)_m=\sum\sum y_iy_j(\alpha a)_{ij};\ \ (\alpha a)_{ij}=\sqrt{(\alpha a)_i(\alpha a)_j}\left(1-k_{ij}\right) \tag{23}$$

where k_{ij} is the binary interaction parameter. Coutinho et al.[31] has proposed a number of values for k_{ij} for CO_2/CH_4 system.

Here, we selected an average value $k_{ij} = k_{ji} = 0.098$ for unlike pairs of molecules, and it is zero for alike pairs of molecules

$$b_m = \sum_i y_i b_i \tag{24}$$

$(AA)_i$ and $(BB)_i$ in Eq. 21 are calculated as

$$(AA)_i = \frac{2}{(a\alpha)_m}\left[\sum_j (a\alpha)_{ij}\right] \tag{25}$$

$$(BB)_i = \frac{b_i}{b_m} \tag{26}$$

Aqueous Thermodynamic. The free energy of the aqueous phase can be written as

$$G_{\mathrm{L}}^{\mathrm{aqueous}} = \sum_{r=c,m,w} x_r \mu_r^{\mathrm{aqueous}} \tag{27}$$

The chemical potential μ_r^{aqueous} for components c (carbon dioxide) and m (methane) dissolved into the aqueous phase is described by nonsymmetric excess thermodynamics

$$\mu_i = \mu_i^{\infty}(T) + RT\ln\left(x_i\gamma_i^{\infty}\right) + v_i^{\infty}(P - P_o) \tag{28}$$

μ_i^{∞} is the chemical potential of component i in water at infinite dilution, γ_i^{∞} is the activity coefficient of component i in the aqueous solution and v_i^{∞} is the partial molar volume of the component i at infinite dilution. The chemical potentials at infinite dilution as a function of temperature are found by assuming equilibrium between fluid and aqueous phases $\mu_i^{Fluid} = \mu_i^{\mathrm{aqueous}}$. This is done at varying low pressures where the solubility is very low and the gas phase is close to ideal gas using experimental values for the solubility and extrapolating the chemical potential down to a corresponding value for zero concentration. The Henry's constants k_{H} are calculated for CH_4 and CO_2 using the expression proposed by Sander[32]

$$k_{\mathrm{H}}(T) = k_{\mathrm{H}}^{\ominus}\mathrm{e}^{\left(\frac{-\Delta_{\mathrm{soln}}H}{R}\left(\frac{1}{T}-\frac{1}{T^{\ominus}}\right)\right)} \tag{29}$$

where $T^{\ominus}$ is the reference temperature, which is equal to 298.15 K. $\Delta_{\mathrm{soln}}H$ is the enthalpy of dissolution, and it is represented by the Clausius–Clapeyron equation[33] as

$$\frac{d\ln k_H}{d(1/T)} = \frac{-\Delta_{\mathrm{soln}}H}{R} \tag{30}$$

The values of $-(d\ \ln[k_H])/d(1/T)$ and $k_{\mathrm{H}}^{\oplus}$ are given by Zheng et al.[34] and by Kavanaugh and Trussell[35] for CO_2 and CH_4, respectively, which is shown in Table 1. The activity coefficient at infinite dilution γ_i^{∞} is calculated as

$$\gamma_i^{\infty} = \frac{f_i^{\infty}}{k_{\mathrm{H}}(T)} \tag{31}$$

where

$$f_i^{\infty} = \mathrm{e}^{\left(-\beta\mu_i^{\infty}\right)}$$

where f_i^{∞} is the fugacity of component i, while μ_i^{∞} is calculated from Ref. 37. The activity coefficient can be regressed using the model for equilibrium to fit experimental solubility data. The chemical potential of water can be written as

$$\mu_w = \mu_w^{\mathrm{pure\ \ liquid}}(T) + RT\ln(1-x)\gamma_w + v_w(P - P_o) \tag{32}$$

where $\mu_w^{\mathrm{pure\ \ liquid}}$ is pure water chemical potential and v_w is the molar volume of water. The strategy for calculating activity coefficient is given by Svandal et al.[36]

Table 1. Values of Parameters

Constants	CO_2	CH_4
$k_{\mathrm{H}}^{\ominus}$ (M/atm)	0.036	0.0013
$-(d\ \ln[k_H])/d(1/T)$(K)	2200	1800

Thermodynamics outside of equilibrium

The PFT model presented in this work have dynamically varying local densities, temperatures and concentrations, and the constraints on the system is the pressure. Unlike our earlier PFT models,[21,51] which were kept at constant temperature, the calculations of nonequilibrium thermodynamic[15] properties are implemented implicit calculations into the PFT model in this version since the free energies of all coexisting phases change dynamically with local conditions and possibly competing phase transitions. We use examples based on conversion of CH_4 hydrate into CO_2 hydrate or mixed CO_2—CH_4 hydrate, which have two primary mechanisms. The first one is that CO_2 creates a new hydrate from free water in the porous media and the released heat dissociate the in situ CH_4 hydrate. This mechanism is primarily dominated by mass-transport rates through fluid phases. A second mechanism is the direct conversion of the in situ CH_4 hydrate with the CO_2, which is a much slower solid-state-phase transition. The first mechanism implies heat release as well as heat consumption and complex coupled behavior of mass and heat transport around the hydrate core is expected. Also note that fluid thermodynamics and aqueous thermodynamics outside of equilibrium is trivial in contrast to hydrate, for which the thermodynamic model is derived from statistical mechanics based on equilibrium between hydrate and fluid phases. For this reason, we expand the thermodynamic properties of hydrate by a first-order Taylor-expansion. This is considered accurate enough since the rate-limiting kinetic contributions are expected to be in the mass transport according to earlier studies.[16,17,35] First of all note that the mass is conserved inside the PFT. The thermodynamics have to be developed in terms of gradients in all directions (P, T, mole-fractions) without conservation of mole-fractions in order to obtain the appropriate relative local driving forces and also avoid double conservation constraints in the free enrgy minimalization. In this article, we limit ourselves to three components, where CH_4 is the additional component to CO_2 and water. This can be directly extended to more components though straightforward extensions of the equilibrium and supersaturation thermodynamics, and appropriate adjustment of the PFT. As the thermodynamic changes are outlined here the primary additional change in the PFT model is in the free energy of the thermal fluctuations[16,37,38] as function of concentrations, which is mathematically trivial. Supersaturations of fluid phases is straightforward and not different from what we have published before[12,16] and in the first part of this article.

The Gibbs free energy of the hydrate phase is written as a sum of the chemical potentials of each component[12,16]

$$G_{\mathrm{H}} = \sum_r x_r \mu_r^{\mathrm{H}} \tag{33}$$

where μ_r^{H} and x_r is chemical potential and mole fraction of component r, respectively. G_{H} is the free energy of hydrate. In the earlier work by Svandal,[16] a simple interpolation in mole-fractions was used between pure CH_4 hydrate and pure CO_2 hydrate, which was considered as sufficient to

theoretically illustrate the exchange concept under PFT. This will of course not reproduce the absolute minimum in free energy for a mixed hydrate in which CH_4 occupies portions of the small cavities and increases stability over pure CO_2 hydrate. The expression for free energy gradients with respect to mole fraction, pressure, and temperature is

$$G_{\mathrm{H}}^{\mathrm{EXP}} = G^{\mathrm{EQ}} + \sum_r \left.\frac{\partial G_{\mathrm{H}}}{\partial x_r}\right|_{P,V,T,x_{i\neq r}} \left(x_r^{\mathrm{act}} - x_r^{\mathrm{EQ}}\right) + \left.\frac{\partial G_{\mathrm{H}}}{\partial P}\right|_{T,V,\vec{x}} \left(P^{\mathrm{act}} - P^{\mathrm{EQ}}\right) + \left.\frac{\partial G_{\mathrm{H}}}{\partial T}\right|_{P,V,\vec{x}} \left(T^{\mathrm{act}} - T^{\mathrm{EQ}}\right) \tag{34}$$

here $G_{\mathrm{H}}^{\mathrm{EXP}}$ is the free energy of hydrate away from equilibrium and the superscripts, EQ and act, represent the corresponding states at equilibrium and actual states, respectively. We are now seeking gradients in all directions, independent of mole-fraction conservation (sum of mole-fractions are conserved inside PFT). So in terms of super saturation in mole-fractions, these have to be evaluated as orthonormal gradient effects. In simple terms that means

$$\frac{\partial x_z}{\partial x_r} = \begin{cases} 0, & z \neq r \\ 1, & z = r \end{cases} \tag{35}$$

where z and r both represent any of the components of the hydrate: water, methane, and carbon dioxide. This is just means that the mole fractions are all independent. Using Eq. 33, we simply take the derivative with respect to one of the mole fractions ($r = m, c$, or w) and the mole fraction derivatives are obtained using Eq. 35 for mole fraction independence, resulting in

$$\frac{\partial G_{\mathrm{H}}}{\partial x_r} = x_c \frac{\partial \mu_c^{\mathrm{H}}}{\partial x_r} + x_m \frac{\partial \mu_m^{\mathrm{H}}}{\partial x_r} + x_w \frac{\partial \mu_w^{\mathrm{H}}}{\partial x_r} + \mu_r \frac{\partial x_r}{\partial x_r} \tag{36}$$

It was previously shown[16] that the chemical potential of a guest molecule can be approximated to a high degree of accuracy and in gradient terms

$$\mu_k^{\mathrm{H}} = A\ln(x_k) + B, \quad \frac{\partial \mu_k^{\mathrm{H}}}{\partial x_r} = \{0, r \neq k\} \tag{37}$$

where k and r both represents any of the components of the hydrate (CO_2, CH_4, and water). For the gradient due to a guest molecule, these simplifications lead to

$$\frac{\partial G_{\mathrm{H}}}{\partial x_k} = x_k \frac{\partial \mu_k^{\mathrm{H}}}{\partial x_k} + \mu_k^{\mathrm{H}} \tag{38}$$

For water, the form has two more terms

$$\frac{\partial G_{\mathrm{H}}}{\partial x_w} = \sum_r x_r \frac{\partial \mu_r^{\mathrm{H}}}{\partial x_w} + \mu_w^{\mathrm{H}} \tag{39}$$

The chemical potential of a guest in the hydrate μ_k^{H} can be written as (Kvamme and Tanaka[8])

$$\mu_k^{\mathrm{H}} = \Delta g_{kj}^{\mathrm{inc}} + RT\ln\left(h_{kj}\right) \tag{40}$$

where $\Delta g_{kj}^{\mathrm{inc}}$ is the Gibbs free energy of inclusion of guest molecule k in cavity j, h_{kj} the cavity partition function of component k in cavity j, the universal gas constant is R and T is temperature. The derivative of Eq. 40 with respect to an arbitrary molecule r is

$$\frac{\partial \mu_k^{\mathrm{H}}}{\partial x_r^{\mathrm{H}}} = \frac{\partial \Delta g_{kj}^{\mathrm{inc}}}{\partial x_r^{\mathrm{H}}} + \frac{\partial\left(RT\ln\left(h_{kj}\right)\right)}{\partial x_r^{\mathrm{H}}} \tag{41}$$

The first term of Eq. 41 is the stabilization energy, which can be evaluated either via the Langmuir constant or using the harmonic oscillator approach.[8] In either case, it can be safely assumed to be a function of only temperature and pressure. Omitting the first term of Eq. 41 and disregarding the impact of guest–guest interactions, one will arrive at

$$\frac{\partial \mu_k^{\mathrm{H}}}{\partial x_r^{\mathrm{H}}} = \frac{RT}{h_{kj}} \frac{\partial h_{kj}}{\partial x_r^{\mathrm{H}}} \tag{42}$$

The wisdom of omitting guest–guest interactions may be questionable in certain cases, even though they are either ignored or empirically corrected for by the majority of hydrate equilibrium codes (the latter can be implemented at a later stage).

The chemical potential of water

$$\mu_w^{\mathrm{H}}\left(T, P, \vec{\theta}\right) = \mu_w^{0,\mathrm{H}}(T, P_0) - \sum_j RT\upsilon_j \ln\left[1 + \sum_k h_{kj}\right] \tag{43}$$

where $\mu_w^{0,\mathrm{H}}$ is the chemical potential of water in an empty hydrate structure, the first sum is taken over both small and a large cavity, the second one is over the components k in the cavity j. Here υ_j is the number of type- j cavities per water molecule. Hydrate structure I contains three large cavities and one small cavity per 23 water molecules, $\upsilon_{\mathrm{l}} = \frac{3}{23}$ and $\upsilon_{\mathrm{s}} = \frac{1}{23}$. The paper by Kvamme and Tanaka[8] provides the empty hydrate chemical potential as polynomials in inverse temperature, the Gibbs free energies of inclusion, and chemical potential of pure water $\mu_w^{\mathrm{pure}}(T)$. The derivative for the above equation with respect to an arbitrary molecule r results in

$$\frac{\partial \mu_w^{\mathrm{H}}}{\partial x_r} = -RT \sum_j \upsilon_j \left[\frac{\sum_k \frac{\partial h_{kj}}{\partial x_r}}{1 + \sum_k h_{kj}}\right] \tag{44}$$

From Eqs. 42 and 44, the derivative of the partition function can be evaluated from the equation that relates the filling fraction to the partition function

$$h_{kj} = \frac{\theta_{kj}}{1 - \sum_i \theta_{ij}} \tag{45}$$

where θ_{kj} is the filling fraction of the components k in the cavity j. But it is easier to recast everything in terms of mole fraction because of the basic assumption of mole fraction independence

$$\theta_{kj} = \frac{x_{kj}}{\upsilon_j x_w} \tag{46}$$

since mass conservation is not used, the usual form of $1 - x_{\mathrm{T}}$ is not considered. This is substituted into Eq. 45 and we get

$$h_{kj} = \frac{x_{kj}}{\upsilon_j x_w - \sum_i x_{ij}} \tag{47}$$

Now we can take the derivative with respect to an arbitrary component r and using Eq. 47, we get

$$\frac{\partial h_{kj}}{\partial x_r} = \frac{h_{kj}}{x_{kj}} \frac{\partial x_{kj}}{\partial x_r} - \frac{h_{kj}^2}{x_{kj}} \left[\upsilon_j \frac{\partial x_w}{\partial x_r} - \sum_i \frac{\partial x_{ij}}{\partial x_r}\right] \tag{48}$$

The first thing that must be dealt with the cavity mole fractions as a function of total mole fraction of a component

$$x_k = \sum_j x_{kj} \tag{49}$$

since the derivative of one mole fraction with respect to another is independent, the mole fraction in the cavity is also independent

$$\left(\frac{\partial x_{kj}}{\partial x_r}\right)=\begin{cases}0, & k\neq r \text{ or } r=w\\ 1, & k=r\end{cases} \tag{50}$$

If $r=w$, then the derivative has to be zero because the mole fraction of the guest are independent of the mole fraction of water. Now Eq. 48 is simplified using Eqs. 49 and 50

$$\frac{\partial h_{kj}}{\partial x_w}=-\frac{h_{kj}^2\upsilon_j}{x_{kj}} \tag{51}$$

$$\frac{\partial h_{kj}}{\partial x_p}=\frac{h_{kj}}{x_{kj}}\frac{\partial x_{kj}}{\partial x_p}+\frac{h_{kj}^2}{x_{kj}}\frac{\partial x_{pj}}{\partial x_p} \tag{52}$$

where p is an arbitrary guest molecule and k is also a guest molecule. These can be the same or different. If k and p are the same molecule, this gradient still exist and the "cross terms" are still able to be found even if there is independency in the mole fractions. $\frac{dx_{kj}}{dx_k}$ is calculated by starting with the Eq. 49, which is the basic definition of the mole fraction of the cavities and how they relate to the total mole fraction of the component. The total methane mole fraction x_m, is the sum of the mole fraction in the large cavities x_{ml}, and the mole fraction in the small cavities x_{ms}

$$x_m=x_{ml}+x_{ms} \tag{53}$$

From discussions, it is assumed that there is a constant ratio between the partition functions and between different cavities of the same component. This is defined as A

$$A\equiv\frac{h_{ml}}{h_{ms}} \tag{54}$$

The partition function can be written in terms of the filling fraction as shown in Eq. 45. Using Eqs. 45, 46, 54 and assuming that the filling fraction of CO_2 in small cavities is zero, we get

$$A\equiv\frac{\frac{x_{ml}}{\upsilon_l x_w}}{\frac{x_{ms}}{\upsilon_s x_w}}\left[\frac{1-\frac{x_{ms}}{\upsilon_s x_w}}{1-\frac{x_{ml}}{\upsilon_l x_w}-\frac{x_{cl}}{\upsilon_l x_w}}\right] \tag{55}$$

This simplifies into

$$x_{ml}[-\upsilon_s x_w]+x_{ms}[A\upsilon_l x_w-Ax_{cl}]+x_{ms}x_{ml}[1-A]=0 \tag{56}$$

Taking derivative of above equation with respect to total methane mole fraction

$$[x_{ms}(1-A)-\upsilon_s x_w]\frac{\partial x_{ml}}{\partial x_m}+[A\upsilon_l x_w-Ax_{cl}+x_{ml}(1-A)]\frac{\partial x_{ms}}{\partial x_m}=0 \tag{57}$$

Substitutions were made to simplify the above equation and get it into a simpler form:

$$\begin{gathered}X=x_{ms}(1-A)-\upsilon_s x_w\\ Y=A\upsilon_l x_w-Ax_{cl}+x_{ml}(1-A)\\ X\frac{\partial x_{ml}}{\partial x_m}+Y\frac{\partial x_{ms}}{\partial x_m}=0\end{gathered} \tag{58}$$

taking the derivative of Eq. 53 with respect to the total mole fraction of methane and simplification results in

$$\begin{gathered}\frac{\partial x_{ml}}{\partial x_m}+\frac{\partial x_{ms}}{\partial x_m}=\frac{\partial x_m}{\partial x_m}=1\\ \frac{\partial x_{ml}}{\partial x_m}=-\frac{Y}{X-Y}\\ \frac{\partial x_{ms}}{\partial x_m}=\frac{X}{X-Y}\end{gathered} \tag{59}$$

substituting the values of X and Y gives the final answer:

$$\begin{gathered}\frac{\partial x_{ml}}{\partial x_m}=-\frac{A\upsilon_l x_w-Ax_{cl}+x_{ml}(1-A)}{x_{ms}(1-A)-\upsilon_s x_w-A\upsilon_l x_w-Ax_{cl}+x_{ml}(1-A)}\\ \frac{\partial x_{ms}}{\partial x_m}=\frac{x_{ms}(1-A)-\upsilon_s x_w}{x_{ms}(1-A)-\upsilon_s x_w-A\upsilon_l x_w-Ax_{cl}+x_{ml}(1-A)}\end{gathered} \tag{60}$$

$\frac{\partial G_H}{\partial P}$ is calculated by taking derivative of Eq. 33 with respect to pressure

$$\frac{\partial G_H}{\partial P}=x_c\frac{\partial \mu_c^H}{\partial P}+x_m\frac{\partial \mu_m^H}{\partial P}+x_w\frac{\partial \mu_w^H}{\partial P}+\mu_c\frac{\partial x_c}{\partial P}+\mu_m\frac{\partial x_m}{\partial P}+\mu_w\frac{\partial x_w}{\partial P} \tag{61}$$

where the chemical potential gradients with respect to pressure can be given by

$$\frac{\partial \mu_r^H}{\partial P}=\bar{V}_r \tag{62}$$

Thus, Eq. 62 can be written as

$$\frac{\partial G_H}{\partial P}=x_c\bar{V}_c+x_m\bar{V}_m+x_w\bar{V}_w+\mu_c^H\frac{\partial x_c}{\partial P}+\mu_m^H\frac{\partial x_m}{\partial P}+\mu_w^H\frac{\partial x_w}{\partial P} \tag{63}$$

The sum of the molar volumes ($\bar{V}_c$, $\bar{V}_m, \bar{V}_w$) is in fact the total clathrate molar volume

$$\bar{V}^{\text{clath}}=x_c.\bar{V}_c+x_m.\bar{V}_m+x_w.\bar{V}_w \tag{64}$$

using the above value of $\bar{V}^{\text{clath}}$ simplifies the Eq. 64 to

$$\frac{\partial G_H}{\partial P}=\bar{V}^{\text{clath}}+\mu_c^H\frac{\partial x_c}{\partial P}+\mu_m^H\frac{\partial x_m}{\partial P}+\mu_w^H\frac{\partial x_w}{\partial P} \tag{65}$$

The mole fraction derivatives can be calculated from EOS but there is no change under this derivative so Eq. 66 can be rewritten as

$$\left[\frac{\partial G_H}{\partial P}\right]_{T,V,\vec{x}}=\bar{V}^{\text{clath}} \tag{66}$$

The free energy gradient with respect to temperature comes from the same fundamental relationship as used for the chemical potential gradient

$$-\frac{\partial}{\partial T}\left[\frac{G}{T}\right]_{P,\vec{x}}=\frac{\bar{H}}{T^2} \tag{67}$$

PFT model

The effects of nonequilibrium thermodynamics on phase transition are incorporated by implementing the thermodynamic model implicitly into phase field simulation. The hydrodynamics effects and variable density were incorporated in a three components PFT by Kvamme et al.[39] through implicit integration of Navier–Stokes equation following the approach of Qasim et al.[14] The basic phase field model for two components is described/used by Wheeler et al.[40] and other references[41–45] and other references therein. The PFT for three components is a straightforward extension of the basic theoretical model. The phase field parameter ϕ is an order parameter describing the phase of the system as a function of spatial and time coordinates. The phase field parameter ϕ is allowed to vary continuously from 0 to 1 on the range from solid to liquid.

The solid state is represented by the hydrate, and the liquid state represents fluid and aqueous phase. The solidification of

hydrate is described in terms of the scalar phase field ϕ (x_1, x_2, x_3) where $x_1, x_2,$ and x_3 represents the molar fractions of CH_4, CO_2, and H_2O, respectively, with obvious constraint on conservation of mass $\sum_{i=1}^{3} x_i = 1$. The field ϕ is a structural order parameter assuming the values $\phi = 0$ in the solid and $\phi = 1$ in the liquid.[16] Intermediate values correspond to the interface between the two phases. The starting point of the three component phase field model is a free energy functional[14]

$$F = \int d\underline{r} \left(\frac{a_\phi^2}{2} T(\nabla\phi)^2 + \sum_{i,j=1}^{3} \frac{a_{xi,j}^2}{4} T\rho(x_i \nabla x_j - x_j \nabla x_i)^2 + f_{\text{bulk}}(\phi, x_1, x_2, x_3, T) \right) \tag{68}$$

which is integration over the system volume, while the subscripts i, j represents the three components, ρ is molar density depending on relative compositions, phase, and flow. The bulk free energy density described as

$$f_{\text{bulk}} = WTg(\phi) + (1 - p(\phi)) f_S(x_1, x_2, x_3, T) + p(\phi) f_L(x_1, x_2, x_3, T) \tag{69}$$

The phase field parameter switches on and off the solid and liquid contributions f_S and f_L through the function $p(\phi) = \phi^3 \left(10 - 15\phi + 6\phi^2\right)$, and note that $p(0) = 0$ and $p(1) = 1$. This function was derived from density functional theory studies of binary alloys and has been adopted also for our system of hydrate-phase transitions. It might be modified by fitting profiles for hydrate/fluid interfaces derived from molecular simulations but for the time being the profile is sufficiently representative. The binary alloys are normally treated as ideal solutions. The free energy densities of solid and liquid is given by

$$f_{\text{bulk}} = WTg(\phi) + (1 - p(\phi)) f_S(x_1, x_2, x_3, T) + p(\phi) f_L(x_1, x_2, x_3, T) \tag{70}$$

$$f_s = G_H \rho_m^H \tag{71}$$

$$f_L = G_L \rho_m^L \tag{72}$$

where the expressions for the free energy of hydrate in a super saturate (or an undersaturated) state as functions of different thermodynamic variables are given through Eqs. 33–68, and the free energies of fluids are described in the first part of the article from some fluid states and in references[36,39,41,42] for other states. The details of densities ρ_m^{hyd} and ρ_m^{L} can be found in Qasim et al.[14] Also note that a possible phase transition will only proceed unconditionally if the free energy change is negative, and more negative than the interface free energy barrier imposed by the interface work needed to give space for the new phase, and also all gradient in free energies results in negative free energy changes for the phase transition. Practically, this latter condition implies that the system is supersaturated with respect to gradients of free energies in all thermodynamically independent variables for the system. If one or more gradients result in positive free energies and the phase transition will compete with other phase transitions.

The function $g(\phi) = \phi^2\left(1 - \phi^2\right)/4$ ensures a double well form of the f_{bulk} with a free energy scale $W = \left(1 - \frac{x_i}{v_m}\right) W_A + \frac{x_i}{v_m} W_B$ with $g(0) = g(1) = 0$, where v_m is the average molar volume of water. In order to derive a kinetic model we assume that the system evolves in time so that its total free energy decreases monotonically.[36,39,41]

The usual equations of motion are supplemented with appropriate convection terms, as explained in Tegze and Grαnαsy[18]; given that the phase field is not a conserved quantity, the simplest form for the time evolution that ensures a minimization of free energy is

$$\frac{\partial\phi}{\partial t} + (\vec{v}.\nabla)\phi = -M_\phi(\phi, x_1, x_2, x_3) \frac{aF}{a\phi} \tag{73}$$

$$\frac{\partial x_i}{\partial t} + (\vec{v}.\nabla) x_i = \nabla.\left(M_{xi}(\phi, x_1, x_2, x_3) \nabla \frac{aF}{axi} \right) \tag{74}$$

where $\vec{v}$ is the velocity, $M_{xi} = x_i(1 - x_i)\frac{1}{RT} D$ and $M_\phi = \left(1 - \frac{x_i}{v_m}\right) M^A + \frac{x_i}{v_m} M^B$ are the mobilities associated with coarse-grained equation of motion which in turn are related to their microscopic counter parts; $D = D_S + (D_L - D_S) p(\phi)$ is the diffusion coefficient. Additional details can be found elsewhere.[16,39]

We have formulated an extended version of the phase field model, which takes into account the effects of fluid flow, density change, and gravity. This is achieved by coupling the time evolution with the Navier–Stokes Equations. The phase and concentration fields associate hydrodynamic equation as described by Conti and coworkers[46–48]

$$\frac{\partial\rho}{\partial t} = -\rho_m \nabla.\vec{v} \tag{75}$$

$$\rho \frac{\partial\vec{v}}{\partial t} + \rho(\vec{v}.\nabla)\vec{v} = \rho\vec{g} + \nabla.P \tag{76}$$

where $\vec{g}$ is the gravitational acceleration. ρ_m is the density of the system in hydrate $\left(\rho_m^{\text{Hyd}}\right)$ and liquid $\left(\rho_m^{\text{L}}\right)$. Further

$$P = \mathfrak{Z} + \Pi \tag{77}$$

is the generalization of stress tensor,[46–48] $\mathfrak{Z}$ represents nondissipative part and Π represents the dissipative part of the stress tensor.

For hydrate formation following water adsorption on rusty walls,[22,23] heat transport is very fast compared to mass transport and not likely to have any significant rate-limiting impact on the kinetic rates. Formation of hydrates inside bulk CO_2 (or inside CO_2/CH_4 fluid) heat-transport rates may have an impact. For these cases, we have so far extended our PFT code according to a simplified scheme as described below.

First consider the general thermodynamic relationship

$$dH = \left(\frac{\partial H}{\partial T}\right)_{P,\vec{x}} dT + \left(V - T\left[\frac{\partial V}{\partial T}\right]_{P,\vec{x}} \right) dp \tag{78}$$

where the molar volume V, as well as the gradient of molar volume with respect to T, is very small for solids and condensed phases. The latter term is also exactly zero for ideal gas. So except for regions of high-pressure gas, the latter term is normally negligible. So for simplicity and also in view of other uncertainties which will be described below the latter term is omitted as an approximation. Strictly speaking, it is not necessary since the volumetric terms are readily available from the solution of the EOS used. The correction could be estimated but the latter term implies couplings to Navier–Stokes that will require some modifications in the integration algorithm.

The two primary contributions to heat transport are conduction and convection. For the systems that we consider, the

conduction term is the dominating. A common approximation in hydrate modeling, as well as in interpretation of experimental data, is therefore, to lump both these contributions into an "apparent" conductivity. Accordingly

$$\dot{Q} = kA\Delta T \tag{79}$$

where k is the "apparent" heat conductivity, A is the area for the heat transport and ΔT the temperature difference. In the integrations of Eqs. 79 and 80, the 2-D or 3-D space in consideration is discretized into grid blocks, and for each grid block, the total molar enthalpy can be written as

$$H_i = (1-\varphi_i)H_{S,i}\left(T,P,\vec{x}_{S,i}\right)+\varphi_i H_{L,i}\left(T,P,\vec{x}_{L,i}\right) \tag{80}$$

where subscript i is the index for grid block number and subscripts S and L denote hydrate and fluid, respectively. These enthalpies are readily available from the individual thermodynamic models involved but are more conveniently evaluated directly from the free energy of each grid block using Eq. 69. From the first law of thermodynamics and combining Eqs. 79 and 80, we arrive at the simple result

$$\left(\frac{\Delta H}{\Delta t}\right)_i = k_i A_i \Delta T_i \tag{81}$$

In discretized form for a chosen time step of the integration, Δt, and corresponding changes in enthalpy and temperature over a time step of progress. A_i is trivially given by the geometry of the grid block system and the dimensions of the system (3-D or 2-D simulation). We make no rigorous discussion on the most appropriate form of an average thermal conductivity of each grid block and have so far implemented the following average value[51]

$$k_i = (1-\varphi_i)k_{S,i}\left(T,P,\vec{x}_{S,i}\right)+\varphi_i k_{L,i}\left(T,P,\vec{x}_{L,i}\right) \tag{82}$$

in which a number of different correlations are available for gas mixtures in the fluid part of the latter term. For liquid water part of the latter term, values are fairly independent of pressure, and since solubility of CO_2 as well CH_4, is limited liquid water provides a fair approximation. Thermal conductivity for hydrate in the solid position of the grid block phase distribution, the value is almost insensitive to both pressures and compositions of the hydrate. Fixed values for $k_{S,i}$ and $k_{L,i}$ are available elsewhere.[52]

Results

The injection of CO_2 into the pore will first displace some of the water surrounding the hydrate due to the minerals normally having a higher thermodynamic affinity for water than hydrate. But this will, of course, depend on the mineral wetting properties. As an example, first few layers of water adsorbed on hematite may have chemical potentials lower by 2–4 kJ/mole than that of liquid water.[13] If the mineral surface is CO_2-wetting, then a greater fraction of the in situ liquid water will surround the hydrate core inside the pores. In this case, the in situ free gas (if existing) will partially dissolve in the injected CO_2. The rate of dissolution will depend on dissolution kinetic rates compared to flow dynamics and rates of CO_2 conversion into hydrate. The rate of CO_2 conversion into hydrate is depends on the diffusion of CO_2 into the porous medium, which would depend on the properties of the medium such as pore sizes, pore connections, and porosity.[53] The 3-D bond pore network model presented by Mu et al.[53] showed that diffusivity increases with mean pore diameter when the pore size is less than 1 μm as a result of the Knudsen effect, with a very strong dependence of effective diffusivity on pore size (which is due to nanoscale to microscale impact of interactions between solid and fluid on energy and entropy generation as well as stress). The increased hydrate formation due to increased diffusion rate of CO_2 into the nanoscale pore size is observed by Adeyemo et al.[54] The relative fraction of water surrounding the hydrate core is of course dependent on several additional factors, but in the example used here for illustration purposes, we have chosen to have water-wetting mineral surface. The degree of water wetting is not important for these examples since thermodynamics of fluids adsorbed on mineral surfaces is not yet implemented but quite feasible along the lines described by Kvamme et al.[21] with additional data on chemical potential of adsorbed water as described by Cuong et al.[22,23] for calcite.

Conversion of CH_4 hydrate over to CO_2 hydrate may proceed via two primary mechanisms. The direct solid-state conversion will be slow, since its rate is related to solid-state diffusivity of CH_4 and CO_2 inside hydrate. The second mechanism implies that injected CO_2 is able to form a new hydrate together with free water surrounding hydrate (and of course also with adsorbed water). Heat released by hydrate formation will contribute to dissociation of in situ CH_4 hydrate. This effect could be expected to enhance the conversion rate as the amount of water surrounding the initial CH_4 hydrate core increases. The larger volume of liquid water around the hydrate would mean greater contact area between it and the CO_2, which would also facilitate the formation of new hydrate. This second mechanism will not be limited by heat transport since the rate of heat transport is 2–3 orders of magnitude faster than that of mass transport[16] through liquid water and hydrate. Conversely, heat transport through the CO_2 phase will be comparatively slow. This factor will, therefore, facilitate heat transfer from the CO_2 hydrate formation region toward the in situ CH_4 hydrate. Liquid-state diffusivity associated with mass transport to and from the hydrate surface will be orders of magnitude faster than the solid-state transport. The second mechanism is, therefore, expected to utterly dominate as long as there is any free water left around the CH_4 hydrate. We, therefore, have considered three different thicknesses of injected CO_2 to study the relative impact.[55]

To save CPU time, simulations are conducted in 2-D although there are no constraints to this in the theory or the PFT code. Two-dimensional is also sufficient for the simple crystal morphology that we are using in our examples at this stage. As mentioned, there are two primary mechanisms involved in the conversion of methane hydrate into a mixed hydrate of carbon dioxide and methane in which some methane will occupy the small cavities. As an approximation, we neglect filling of carbon dioxide in the small cavities since it is so far uncertain if this will be significant for rapid phase transitions in a dynamic reservoir flow environment. The thermodynamic stabilization from CO_2 filling in large is also uncertain since the cavity partition functions for CO_2 in small cavities are extremely small and in molecular dynamics simulations, using different well-known interaction models for CO_2, the hydrate dissociates fast. These are so far unpublished results. So even though experimental evidence may suggest that CO_2 might be trapped in small cavities, it does not necessary imply that chemical potential of hydrate water will be lowered by this occupancy. On the contrary, it might even result in large

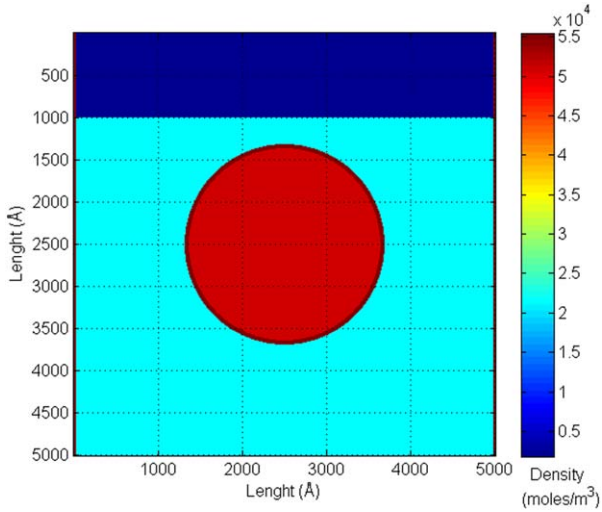

Figure 1. Initial snapshot of density (moles/m^3) profile shows the initial distribution of phases and components for (5000 Å × 5000 Å) system; red disk in the center is CH_4 hydrate core, water regions are represented by maroon color, dark blue region is methane, and rest is CO_2, Similar distribution for other two 2-D systems.

[Color figure can be viewed in the online issue, which is available at wileyonlinelibrary.com.]

CO_2 molecule hindering water liberations. Even a spherical CO_2 model in large cavity will interfere with some water liberational frequencies.[8] The chemical potential for water is roughly 1 kJ/mole at 273 K higher when water movement is accounted for by molecular dynamics simulations compared to the Langmuir constant integration using a fixed water lattice.[8] The difference is likely to be substantially worse for the small cavity. So given that it is uncertain if CO_2 is actually trapped in small cavities in significant amounts under the dynamic situations, we focus on we approximate to zero filling of CO_2 in small cavities.

The three 2-D systems of size 5000 Å × 5000 Å representing the sample pores size. The initial hydrate saturation was same for all systems, with hydrate cores represented by disks of radius 1136 Å located at the center of the 2D systems. The initial pure methane saturation is approximately 20% of the pore area. Water strips of varying thickness (5, 50, and 70 Å) are introduced around the hydrate core, with the rest of the system saturated with CO_2 to represent two different amounts of free water surrounding the hydrate and corresponding different water/CO_2 contact areas. A sample system is shown in Figure 1.

The distribution of phases and components shown in Figure 1 is based on average liquid water saturation, free gas saturation, and hydrate saturation of a real reservoir. Thickness of water film around the hydrate core shown in Figure 1 is 50 Å as an example. The model pore is a square shape of size 5000 Å × 5000 Å in Figure 1 and sI Structure hydrate is represented by circular region in red color right in center of the pore. The water saturation is represented with maroon color around hydrate in addition to the two strips adjacent to the walls. Considering the injection of CO_2 has moved methane up from its original position around the hydrate is, therefore, represented by the upper dark blue strip. The rest of the region shows the injected CO_2. The pressure is kept constant at 83 bars and the initial temperature is uniform and 277.15 K. These conditions have been used in this initial study since these conditions were applied in a number of experiments conducted in ConocoPhillips laboratory in Bartlesville over more than a decade. See for instance Kvamme and coworkers,[19,21] for examples and description of the experimental setup. Comparison with these experimental data will also require inclusion of realistic mineral surfaces, and that is a future goal.

The existence of free water and CO_2 liquid form a new CO_2 hydrate and as a result releases heat as shown in Figure 2. Heat released here is a dominating factor in the fast initial dissociation of methane hydrate and as a result allowing a faster initial exchange process. The second, dominating factor in the initial dissociation process is the lower energy state of CO_2 as the guest molecule in sI gas hydrate structures vs. CH_4. This results in more favorable thermodynamics conditions of formation for the pure CO_2 vs. pure CH_4 hydrates over large regions of pressures and temperatures, while mixed hydrate in which CO_2 dominates occupation of large cavities and CH_4

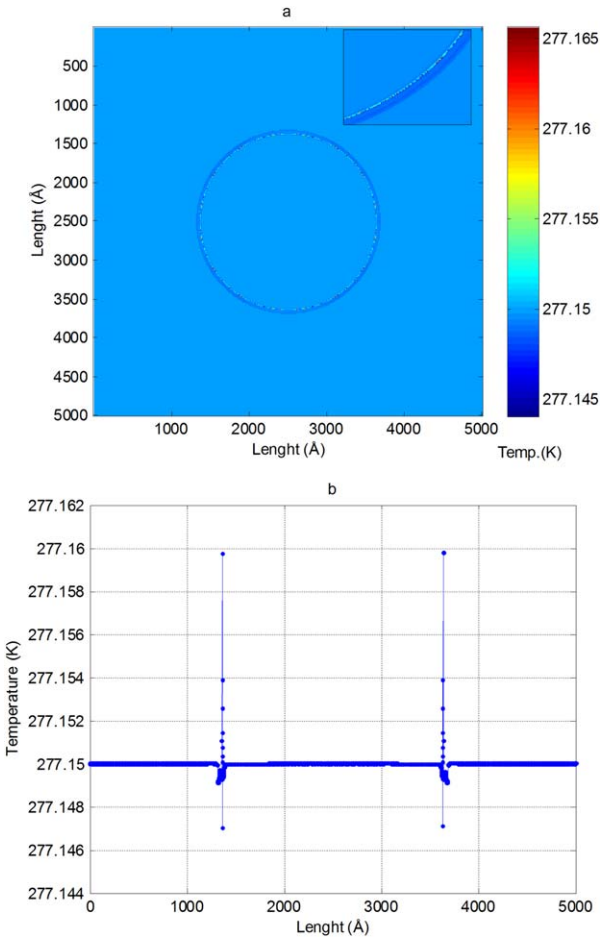

Figure 2. (a) Snapshot of temperature in kelvin shows an increased around the CH_4 hydrate due to formation of CO_2 hydrate, color bar is associated with (a) representing temperature in kelvin. For a more clear insight, a region at interface is highlighted and zoomed in. (b) Temperature curve from one end to another passing through center of CH_4 hydrate.

[Color figure can be viewed in the online issue, which is available at wileyonlinelibrary.com.]

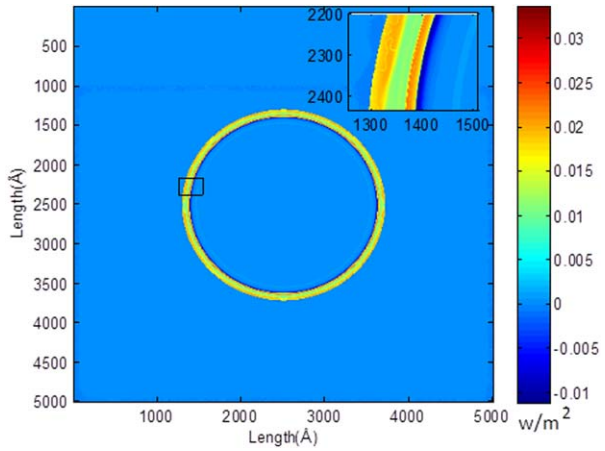

Figure 3. Heat flux profile.

[Color figure can be viewed in the online issue, which is available at wileyonlinelibrary.com.]

dominates occupation of small cavities is more stable at all conditions of temperature and pressure.

The formation of hydrate is an exothermic process and, therefore, result an increase in temperature in the area of new CO_2 hydrate formation, as shown in Figure 2a. Heat transport through CO_2 region is slow which will, therefore, also facilitate the heat being transported from the CO_2 hydrate formation region toward the in situ CH_4 hydrate as shown in Figure 3. The calculation details are given in Appendix.

The encircled region in Figure 2a is also show gaps in the increasing temperature regions at the interface which are typically escape regions for dissociating methane mainly from the large cavities of hydrate. The dissociation extracts heat since it is an endothermic process. Hydrate dissociation extracts heat from the surroundings which is illustrated in Figures 2a, b by regions of reduced temperature.

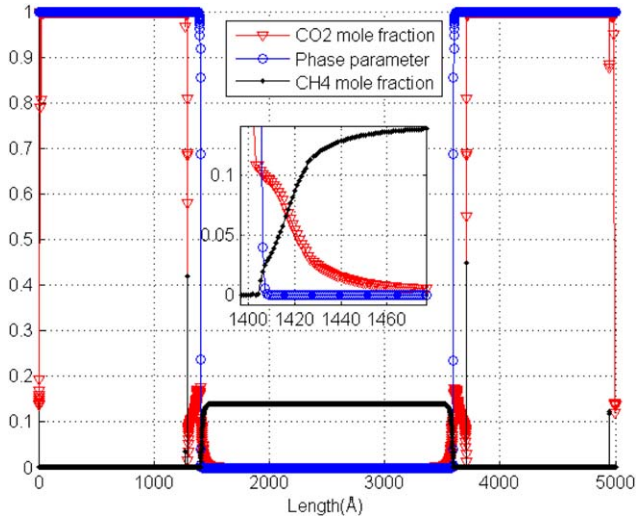

Figure 4. CO_2 filling in hydrate while curve of methane mole fraction shows dissociation of methane, phase parameter curve to indicate hydrate and fluid phases.

The zoomed graph is showing the clear picture of exchange process. [Color figure can be viewed in the online issue, which is available at wileyonlinelibrary.com.]

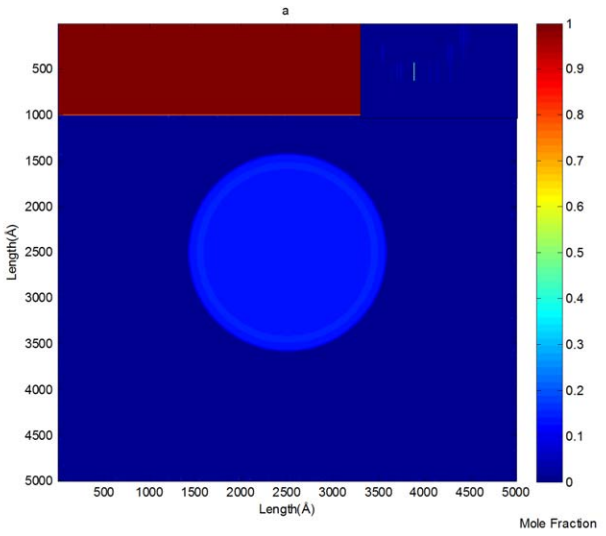

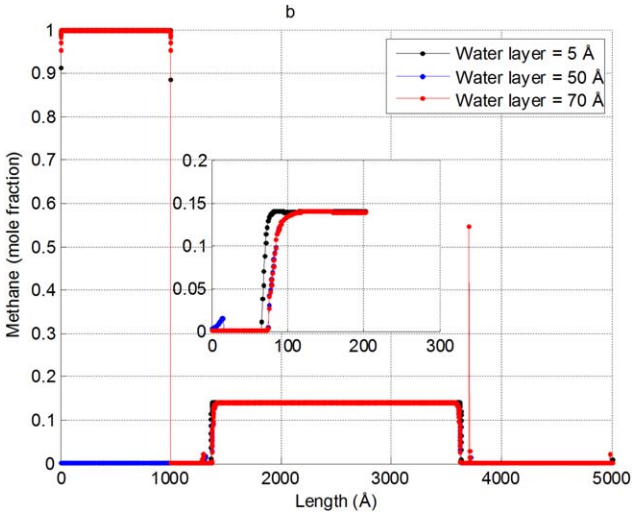

Figure 5. Snapshot of methane mole fraction in entire system after 4.84 ns.

(a) Methane mole fraction across the system after 4.84 ns for the system with water thickness 70 Å. A region at the interface is highlighted and zoomed in to show methane as free gas. (b) A comparison of methane mole fraction after 4.84 ns of three examples. [Color figure can be viewed in the online issue, which is available at wileyonlinelibrary.com.]

All the curves in Figure 4 and in coming figures show variation in parameters along the line starting from the boundary of the 2-D geometry in Figure 1 adjacent to blue methane region to the opposite boundary passing through the center of hydrate. This will show the variation in parameters in the pore with a single curve. The CO_2, CH_4 concentrations, and phase field curves in Figure 4 show that CO_2 has converted the interface water layer into hydrate and created a new interface dominated by CO_2 in favor of CH_4 with water and then started the (slow) solid-state conversion of the CH_4 hydrate core. The phase parameter is represented by the third curve in Figure 4 is drawn here to show precisely the changes in mole fraction of CO_2 and CH_4 inside hydrate.

Due to dissolution kinetics, the surrounding CO_2 will not be able to dissolve the released methane within the time window of simulation time. Methane will, therefore, exist as free gas bubbles near the interface and then gradually increasing in

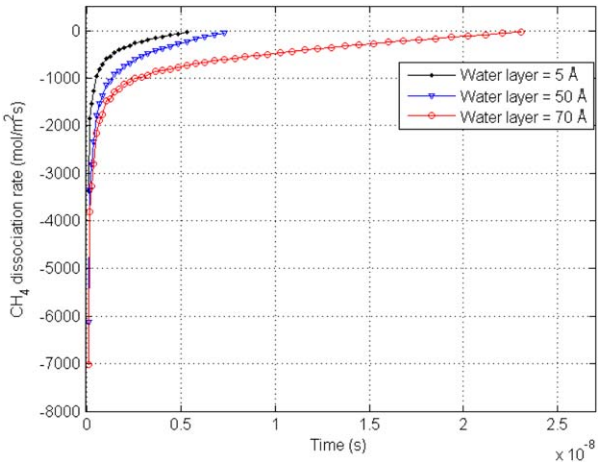

Figure 6. A comparison of estimated methane release rate in three systems.

[Color figure can be viewed in the online issue, which is available at wileyonlinelibrary.com.]

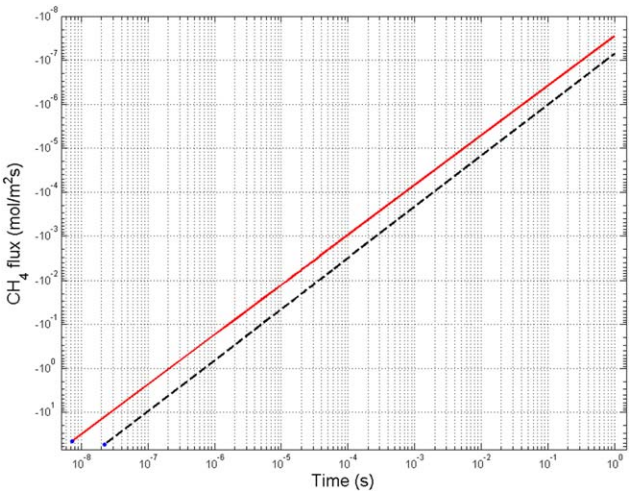

Figure 7. Extrapolation of CH_4 flux into experimental time-scale.

The solid red line represents simulation with 50-Å water thickness and dashed black line is for simulation with 70-Å water thickness around hydrate core. [Color figure can be viewed in the online issue, which is available at wileyonlinelibrary.com.]

CO_2 content. CH_4 and CO_2 are mutually soluble at these conditions according to the thermodynamics but there are constraints on the solubility kinetics in terms of diffusivities compared to the impact of Navier–Stokes on the local variations in densities. The existence of free CH_4-dominated gas bubbles from released CH_4 can be observed in this example as shown in Figure 5. Some few regions of free gas are particularly expressed by encircling them within the fluid phase in Figure 5. The mole fraction of methane in those regions varies in the range of 0.4–0.65. The system with the larger water layer thickness around initial hydrate has more methane at interface after a particular simulation time. The larger water layer ensures a higher dissociation rate of methane from hydrate due to a larger amount of new CO_2 hydrate being formed per unit time and rapid heat transport inward toward the hydrate core and slow heat transport into surrounding CO_2 phase. A comparison of dissociation rates of methane is presented in Figure 6 to emphasize this picture.

The simulation results covered a limited time interval due to computational restrictions, with only a fraction of the large cavities being filled with CO_2. Achieving a full exchange will require substantially longer simulation runs even when using a supercomputer with relatively high parallelization. The rate of CH_4 release, as illustrated in Figure 6, clearly shows that methane was still being released even toward the end of the simulations, though with the rate did decrease as the amount of free liquid water diminished due to transition to the slow solid-state exchange mechanism. All of the systems appear to enter a stationary slow progress dominated by solid-state exchange. To illustrate this, the numeric results were extrapolated to experimental time as the interface in these simulations is perfectly follows the power law, which is proportional to square root of time showing a diffusion control process (Figure 7). The dissociation rate by second mechanism is orders of magnitude faster than solid-state transport, which is illustrated in Table 2.

As expected, a system with the thinnest liquid water layer entered the slow-exchange stage faster than systems with more free water available to create new CO_2 hydrate. The difference in transition of rates between the heat supply mechanism vs. the solid-state transport is illustrated in Figure 8. These results will have significant practical implications; the conclusion that initial saturation of free water capable of producing new CO_2 hydrate will be a critical dynamic factor for conversion of in situ CH_4 hydrate into CO_2 and mixed CO_2/CH_4 hydrate being of utmost importance. And since the rate of heat absorption related to dissociation of CH_4 hydrate will be controlled and rate-limited by mass transport across the liquid water/hydrate interface, there will be a kinetic balance involved as well. Given that it is the interface that provides the most favorable site for hydrate formation from injected CO_2 and pore water, pore blockage can occur fast due to relatively thin but mechanically strong interface hydrates will potentially be able to trap liquid water and CO_2. This impact can be reduced by several additives. The high hydrate saturations typical for Alaska may, therefore, not be ideal for the conversion method, although CO_2/N_2 injection will work (Ignik Sikumi gas hydrate field trial[26]) and would perform better with a different completion type (separate injection and production wells) since the CH_4—CO_2—nitrogen exchange will result in a beneficent gas density gradient between injection and production sites.

Conclusions

The exchange of CH_4 with CO_2 in the hydrate will be controlled by two primary mechanisms. The fastest one will involve creation of new CO_2 hydrate. This new hydrate can nucleate from phases adsorbed on mineral surfaces, existing

Table 2. CH_4 Dissociation Rates

	Simulation 2 with water thickness 50 Å		Simulation 3 with water thickness 70 Å	
Time (s)	1.6 e −010	1	1.6 e −010	1
Dissociation rates (mol/m^{2}s)	3.365 e +003	2.858 e −008	3.815 e +003	7.249 e −008

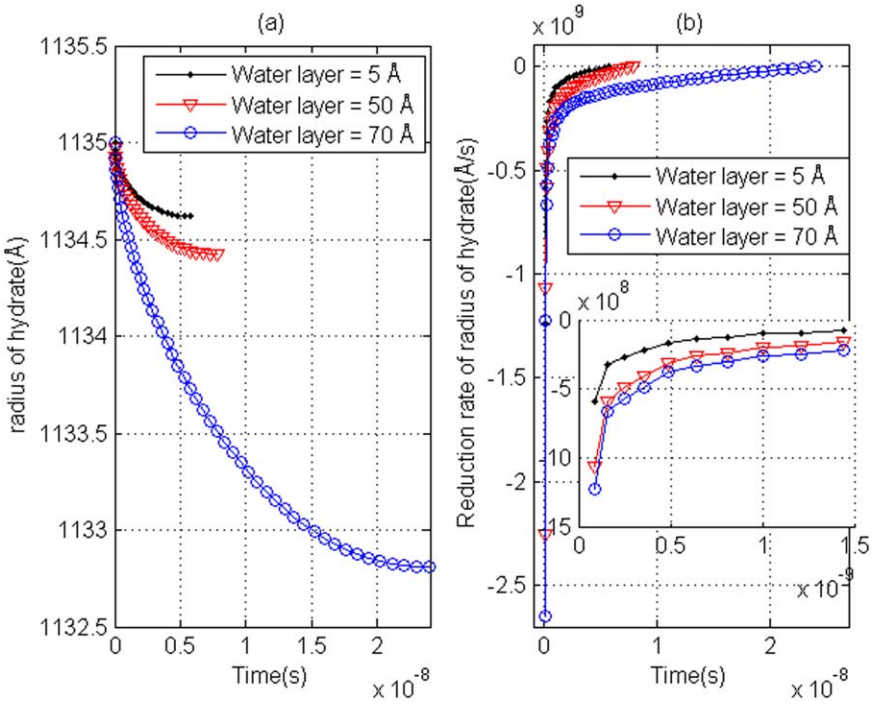

Figure 8. Development of the mix CH_4/CO_2 hydrate core as function of time three examples.

(a) Radius as function of time and (b) rate of radius reduction as function of time. [Color figure can be viewed in the online issue, which is available at wileyonlinelibrary.com.]

hydrate, or interface between liquid water and CO_2. Heat released by hydrate created from water surrounding the hydrate core will be mainly transported through water and existing hydrate since the surrounding CO_2 can be considered a thermal insulator, given its heat-transport rate is extremely small compared to liquid water and hydrate. In practice, this would mean that kinetic rate of this mechanism will be determined by the rate of liquid-state mass transport. This will be in contrast to a second, much slower mechanism, whose rate is proprotional to that of solid-state transport of molecules through hydrate.

We have applied a PFT developed and discussed in more detail through our previous studies[14–21] to investigate and analyze these complex hydrate phase transitions. Three examples of square 2-D model systems identical in size (5000 Å × 5000 Å) and having the same initial spherical CH_4 hydrate core (radius of 1136 Å) but differing in water film thickness around the hydrate core have been simulated to illustrate our approach. The initial conversion process has proven to be fast in all three systems as expected, since this stage is dominated by rapid formation of new CO_2 hydrate and subsequent dissociation of CH_4 hydrate facilitated by released heat of formation. The thickness of the water film was shown to strongly affect the rate of exchange, which increased with the thickness. The availability of free water facilitates the formation of new CO_2 hydrate, which results in release of heat and, therefore, promotes a faster dissociation of initial CH_4 hydrate core, eventually raising the exchange rate. After the free water has been consumed, the exchange rate is governed by solid-state transport, with all three systems observed to reach the same asymptotic limit accordingly.

ACKNOWLEDGMENTS

The authors acknowledge the grant and support from Research Council of Norway through the following projects: SSC-Ramore, "Subsurface storage of CO_2 - Risk assessment, monitoring and remediation", Research Council of Norway, project number: 178008/I30, FME-SUCCESS, Research Council of Norway, project number: 804831, PETROMAKS, "CO_2 injection for extra production", Research Council of Norway, project number: 801445, STATOIL through contract 4502354080 and Research Council of Norway, project number: 224857.

Literature Cited

1. Tsuji Y, Fujii T, Hayashi M, Kitamura R, Nakamizu M, Ohbi K, Saeki T, Yamamoto K, Namikawa T, Inamori T, Oikawa N, Shimizu S, Kawasaki M, Nagakubo S, Matsushima J, Ochiai K, Okui T. Methane-hydrate occurrence and distribution in the eastern Nankai trough, Japan: findings of the Tokai-oki to Kumano-nada methane-hydrate drilling program. In: T. Collett, A. Johnson, C. Knapp, and R. Boswell, editors. *Natural Gas Hydrates – Energy Resource Potential and Associated Geologic Hazards*. AAPG Memoir 89. 2009:228–249.
2. Boswell R, Collett TS. Current perspectives on gas hydrate resources. *Energy Environ Sci*. 2011;4:1206–1215.
3. Boswell R, Collett T, McConnell D, Frye M, Shedd B, Mrozewski S, Guerin G, Cook A, Godfriaux P, Dufrene R, Roy R, Jones E. *Joint Industry Project Leg II Discovers Rich Gas Hydrate Accumulations in Sand Reservoirs in the Gulf of Mexico, Fire in the Ice*, US Department of Energy, Office of Fossil Energy. National Energy Technology Laboratory. 2009;9:1–5.
4. Lee MW, Collett TS. In-situ gas hydrate hydrate saturation estimated from various well logs at the Mount Elbert Gas Hydrate Stratigraphic Test Well, Alaska North Slope. *Mar Petroleum Geol*. 2011;28:439–449.
5. Torres ME, Collett T, Rose K, Sample JC, Agena W, Rosenbaum E. Pore fluid geochemistry from the Mount Elbert Gas Hydrate Stratigraphic Test Well, Alaska North Slope. *Mar Petroleum Geol*. 2011;28:332–342.
6. Dai S, Lee C, Santamarina JC. Formation history and physical properties of sediments from the Mount Elbert Gas Hydrate Stratigraphic Test Well, Alaska North Slope. *Mar Petroleum Geol*. 2011;28:427–438.
7. Michael DM, Arthur HJ, Villiam PD. *Economic Geology of Natural Gas Hydrate*. Dordrecht: Springer, 2006.
8. Kvamme B, Tanaka H. Thermodynamic stability of hydrates for ethane, ethylene, and carbon dioxide. *J Phys Chem*. 1995;99:7114–7119.

9. Shpakov VP, Tse JS, Kvamme B, Belosludov VR. Elastic moduli calculation and instability in structure I methane clathrate hydrate. *Chem Phys Lett*. 1998;282:107–114.
10. Koh C, Sloan ED. *Clathrate Hydrates of Natural Gases; Chemical Industries*, 3rd ed. CRC Press/Taylor & Francis, 2008.
11. Kvamme B. Initiation and growth of hydrate from nucleation theory. *Int J Offshore Polar Eng*. 2002;12:256–262.
12. Kvamme B. Droplets of dry ice and cold liquid CO_2 for self transport to large depths. *Int J Offshore Polar Eng*. 2003;13:1–8.
13. Kvamme B, Kuznetsova T, Kivelæ PH. Adsorption of water and carbon dioxide on Hematite and consequences for possible hydrate formation. *Phys Chem Chem Phys*. 2012;14:4410–4424.
14. Qasim M, Kvamme B, Baig K. Phase field theory modeling of CH_4/CO_2 gas hydrates in gravity fields. *Int J Geol*. 2011;5:48–52.
15. Kvamme B, Baig K, Qasim M, Bauman J. Thermodynamic and kinetic modeling of CH_4/CO_2 hydrates phase transitions. *Int J Energy Environ*. 2013;7:1–8.
16. Svandal A. Modeling Hydrate Phase Transitions Using Mean-field Approaches, PhD Thesis, University of Bergen, 2006.
17. Kvamme B, Svandal A, Buanes T, Kuznetsova T. Phase field approaches to the kinetic modeling of hydrate phase transitions. *AAPG Memoir*. 2009;89:758–769.
18. Tegze G, Grønæsy L. Phase field simulation of liquid phase separation with fluid flow. *Mater Sci Eng*. 2005;413–414:418–422.
19. Kvamme B, Graue A, Aspenes E, Kuznetsova T, Grønæsy L, Tóth G, Pusztai T, Tegze G. Kinetics of solid hydrate formation by carbon dioxide: phase field theory of hydrate nucleation and magnetic resonance imaging. *Phys Chem Chem Phys*. 2004;6:2327–2334.
20. Tegze G, Grønæsy L, Kvamme B. Phase field modeling of CH_4 hydrate conversion into CO_2 hydrate in the presence of liquid CO_2. *Phys Chem Chem Phys*. 2007;9:3104–3111.
21. Kvamme B, Graue A, Buanes T, Kuznetsova T, Ersland G. Storage of CO_2 in natural gas hydrate reservoirs and the effect of hydrate as an extra sealing in cold aquifers. *Int J Greenhouse Gas Control*. 2007;1:236–246.
22. Cuong PV, Kvamme B, Kuznetsova T, Jensen B. The impact of short-range force field parameters and temperature effect on selective adsorption of water and CO_2 on calcite. *Int J Energy Environ*. 2012;6:301–309.
23. Cuong PV, Kvamme B, Kuznetsova T, Jensen B. Molecular dynamics study of calcite and temperature effect on CO_2 transport and adsorption stability in geological formations. *Mol Phys*. 2012;110:1097–1106.
24. Lee H, Seo Y, Seo YT, Moudrakovski IL, Ripmeester JA. Recovering methane from solid methane hydrate with carbon dioxide. *Angew Chem Int Ed*. 2003;42:5048–5051.
25. Kuznetsova T, Kvamme B, Morrissey K. An alternative for carbon dioxide emission mitigation: in situ methane hydrate conversion. *AIP Conf Proc*. 2012;1504:772–775.
26. The U.S. Department of Energy's National Energy Technology Laboratory (NETL). Ignik Sikumi Gas Hydrate Field Trial 2012. Available at: http://www.netl.doe.gov/research/oil-and-gas/methane-hydrates/co2_ch4exchange. Accessed September 25, 2014.
27. van der Waals JH, Platteeuw JC. Clathrate solutions. *Adv Chem Phys*. 1959;2:1–57.
28. Reid RC, Prausnitz JM, Sherwood TK. *The Properties of Gases and Liquids*, 3rd ed. McGraw-Hill, 1977.
29. Kvamme B, Kuznetsova T, Kivelæ PH, Bauman J. Can hydrate form in carbon dioxide from dissolved water? *Phys Chem Chem Phys*. 2013;15:2063–2074.
30. Soave G. Equilibrium constants from a modified Redlich-Kwong equation of state. *Chem Eng Sci*. 1972;27:1197–1203.
31. Coutinho JAP, Kontogeorgis GM, Stenby EH. Binary interaction parameters for nonpolar systems with cubic equations of state—a theoretical approach. 1. CO_2 hydrocarbons using SRK equation of state. *Fluid Phase Equilib*. 1994;102:31–60.
32. Sander R. Modeling atmospheric chemistry: interactions between gas-phase species and liquid cloud/aerosols particles. *Surv Geophys*. 1999;20:1–31.
33. Li JCM. Clapeyron equation for multicomponent systems. *J Chem Phys*. 1956;25:572–574.
34. Zheng DQ, Guo TM, Knapp H. Experimental and modeling studies on the solubility of CO_2, $CHCLF_2$, CHF_3, $C_2H_2F_4$ and $C_2H_4F_2$ in water and aqueous NACL solutions under low-pressures. *Fluid Phase Equilib*. 1997;129:197–209.
35. Kavanaugh MC, Trussell RR. Design of aeration towers to strip volatile contaminants from drinking water. *J Am Water Works Assoc*. 1980;72:684–692.
36. Svandal A, Kuznetsova T, Kvamme B. Thermodynamic properties and phase transitions in the H2O/CO2/CH4 system. *Fluid Phase Equilib*. 2006;246:177–184.
37. Conti M. Solidification of binary alloys: thermal effects studied with the phase-field model. *Phys Rev A*. 1997;55:765–771.
38. Conti M. Thermal and chemical diffusion in the rapid solidification of binary alloys. *Phys Rev E*. 2000;61:642–650.
39. Kvamme B, Svandal A, Buanes T, Kuznetsova T. *Phase Field Approaches to the Kinetic Modeling of Hydrate Phase Transitions*, Vancouver, BC, Canada, September 12–16, 2004.
40. Wheeler AA, Boethinger WJ, McFadden GB. Phase field model for isothermal phase transitions in binary alloys. *Phys Rev A*. 1992;45:7424–7439.
41. Gránásy L, Pusztai T, Jurek Z, Conti M, Kvamme B. Phase field theory of nucleation in the hard sphere liquid. *J Chem Phys*. 2003;119:10376–10382.
42. Gránásy L, Pusztai T, Börzsönyi T, Warren JA, Kvamme B, James PF. Nucleation and polycrystalline solidification in binary phase field theory. *Phys Chem Glasses*. 2004;45:107 - 115.
43. Tegze G, Pusztai T, Tóth G., Gránásy L, Svandal A, Buanes T, Kuznetsova T, Kvamme B. Multiscale approach to CO_2 hydrate formation in aqueous solution: phase field theory and molecular dynamics. Nucleation and growth. *J Chem Phys*. 2006;124:234710.
44. Gránásy L, Börzsönyi T, Pusztai T. Nucleation and bulk crystallization in binary phase field theory. *Phys Rev Lett*. 2002;88:206105–206108.
45. Gránásy L, Pusztai T. Diffuse interface analysis of crystal nucleation in hard-sphere liquid. *J Chem Phys*. 2002;117:10121–10124.
46. M. Conti. Density change effects on crystal growth from the melt. *Phys Rev E*. 2001;64:051601.
47. Conti M, Fermani M. Interface dynamics and solute trapping in alloy solidification with density change. *Phys Rev E*. 2003;67:026117.
48. Conti M. Advection flow effects in the growth of a free dendrite. *Phys Rev E*. 2004;69:022601.
49. Circone S, Stern LA, Kirby SH, Durham WB, Chakoumakos BC, Rawn CJ, Rondinone AJ, Ishii Y. CO_2 hydrate: synthesis, composition, structure, dissociation behavior, and a comparison to structure I CH_4 hydrate; Lawrence Livermore National Laboratory. *J Phys Chem*. 2003;107:5529–5539.
50. Qasim M, Baig K, Kvamme B, Bauman J. Mix hydrate formation by CH_4-CO_2 exchange using phase field theory with implicit thermodynamics. *Int J Energy Environ*. 2012;6:479–487.
51. Qasim M. Microscale Modeling of Natural Gas Hydrates in Reservoirs, PhD Thesis, University of Bergen, 2013.
52. Haq BU. 1998. Natural gas hydrates: searching for the long-term climatic and slope-stability records. In: J.-P. Henriet and J. Mienert, editors. *Gas Hydrates: Relevance to World Margin Stability and Climate Change. Geological Society*, London, Special Publications, 137:303–318.
53. Mu D, Liu ZS, Huang C, Djilali N. Determination of the effective diffusion coefficient in porous media including Knudsen effects. *Microfluidics Nanofluidics*. 2008;4:257–260.
54. Adeyemo A, Kumar R, Linga P, Ripmeester J, Englezos P. Capture of carbon dioxide from flue or fuel gas mixtures by clathrate crystallization in a silica gel column. *Int J Greenhouse Gas Control*. 2010;4:478–485.
55. Kvamme B, Qasim M, Baig K, Kivelä PH, Bauman J. Hydrate phase transition kinetics from phase field theory with implicit hydrodynamics and heat transport. *Int J Greenhouse Gas Control*. 2014;29:263–278.
56. Asgeirsson LS, Ghajar AJ. Prediction of thermal conductivity and viscosity for some fluids in the near-critical region. *Chem Eng Commun*. 1986;43:165–184.
57. Sharqawy MH, Lienhard VJH, Zubair SM. Thermophysical properties of seawater: a review of existing correlations and data. *Desalination Water Treat*. 2010;16:354–380.
58. Todd B, Young JB. Thermodynamic and transport properties of gases for use in solid oxide fuel cell modelling. *J Power Sources*. 2002;110:186–200.

Appendix

Heat flux profile is calculated using the conduction equation:

$$\frac{q}{A} = -k\Delta T$$

$$\vec{q} = -(T_{t+dt} - T_t)\sum\nolimits_{i=\mathrm{CH_4},\mathrm{CO_2},\&\mathrm{water}} x_i k_i$$

where $\vec{q}$ is the heat flux in units W/m^2. k_i is the thermal conductivity of component i in W/mK and subscript i represents

components CO_2, CH_4, and H_2O. ΔT is the change in temperature at different time in kelvin (K) and x_i is the mole fraction of component i and subscript i represents components CO_2, CH_4, and H_2O.

A1: Thermal conductivity of liquid CO_2[56]

$$k_{CO_2} = a_1 + b_1\rho + c_1\rho^2 + d_1\rho^3 + e_1\left[T^*\left(1 + \frac{0.9\rho^{*2.86}}{T^*}\right)\right]^{-0.6}\rho_r^{0.5} \quad \text{(A1)}$$

where

$$a_1 = -4.406180\times10^{-2}$$
$$b_1 = 5.981447\times10^{-4}$$
$$c_1 = -1.331925\times10^{-6}$$
$$d_1 = 1.022006\times10^{-9}$$
$$e_1 = 2.739334\times10^{-3}$$
$$T^* = \left|\frac{T - T_c}{T_c}\right|$$
$$\rho^* = \left|\frac{\rho - \rho_c}{\rho_c}\right|$$

T, is the temperature in kelvin (K)
The critical temperature of CO_2, $T_C = 304.21\ (K)$
The critical density of CO_2, $\rho_c = 4.64\times10^2\left(\frac{kg}{m^3}\right)$
The reduced density, $\rho_r = 0.95$,
ρ, is the liquid CO_2 density in kg/m^3

A2: Thermal conductivity of pure water[58]

$$k_{H_2O} = \sum_{i=1}^{4} a_i\left(\frac{T}{300}\right)^{b_i} \quad \text{(A2)}$$

where

$$a_1 = 0.80201$$
$$a_2 = -0.25992$$
$$a_3 = 0.10024$$
$$a_4 = -0.032005$$
$$b_1 = -0.32$$
$$b_2 = -5.7$$
$$b_3 = -12$$
$$b_4 = -15$$

T, is the temperature in kelvin (K)

A3: Thermal conductivity of CH_4[58]

$$k_{CH_4} = 0.01\sum_{i=0}^{6} c_i\tau^i \quad \text{(A3)}$$

where

$$c_0 = 0.4796$$
$$c_1 = 1.8732$$
$$c_2 = 37.413$$
$$c_3 = -47.440$$
$$c_4 = 38.251$$
$$c_5 = -17.283$$
$$c_6 = 3.2774$$
$$\tau = \frac{T}{1000}$$

T, is the temperature in kelvin (K)

Manuscript received Sep. 29, 2014, and revision received May 7, 2015.